

Saturated flow boiling heat transfer of R-407C and associated bubble characteristics in a narrow annular duct

F.C. Hsieh, K.W. Li, Y.M. Lie, C.A. Chen, T.F. Lin *

Department of Mechanical Engineering, National Chiao Tung University, Hsinchu 30010, Taiwan, ROC

Received 4 October 2007; received in revised form 10 January 2008

Available online 7 March 2008

Abstract

Experiments are conducted here to investigate how the channel size affects the R-407C saturated flow boiling heat transfer and associated bubble characteristics in a horizontal narrow annular duct. The gap of the duct is fixed at 1.0 and 2.0 mm in this study. The measured data indicate that the saturated flow boiling heat transfer coefficient increases with a decrease in the duct gap. Besides, raising the imposed heat flux can cause a significant increase in the boiling heat transfer coefficients. However, the effects of the refrigerant mass flux and saturated temperature on the boiling heat transfer coefficient are milder. The results from the flow visualization show that the mean diameter of the bubbles departing from the heating surface decreases noticeably at increasing R-407C mass flux. Moreover, the bubble departure frequency increases at reducing duct size and at a high imposed heat flux many bubbles generated from the cavities in the heating surface tend to merge together to form big bubbles. Meanwhile comparison of the present heat transfer data for R-407C with R-134a in the same duct and with some existing correlations is conducted. Furthermore, correlation for the present R-407C saturated flow boiling heat transfer data is proposed. Additionally, the present data for some quantitative bubble characteristics such as the mean bubble departure diameter and frequency and the active nucleation site density are also correlated.

© 2008 Elsevier Ltd. All rights reserved.

1. Introduction

In the air conditioning and refrigeration system design the choice of refrigerant is known to play an important role. Besides, the production of the chlorofluorocarbons refrigerants (CFCs) has been prohibited since 1996 and the hydrochlorofluorocarbons refrigerants (HCFCs) are going to be phased out in 2020, due to the presence of chlorine and carbon in these refrigerants which were found to destruct the ozone layer in the outer atmosphere around the earth and to increase the total equivalent warming impact (TEWI). Thus, the search for the replacement of CFCs and HCFCs becomes urgent recently. The hydrofluorocarbons refrigerants (HFCs) such as R-134a, R-407C, R-410a, R-410b and R-507 have been considered to be suitable and some are currently in use.

To enhance the boiling and condensation heat transfer performance, small channel with its small volume, lower total mass and low inventory of working fluids is a good choice for the compact heat exchangers used in air conditioning and refrigeration systems. The understanding of boiling and condensation heat transfer and flow characteristics in the small channels consisted in compact heat exchangers are therefore very important. The size of channels in a compact heat exchanger can significantly affect the performance of the exchanger. In sizing the small channels, Kandlikar and Grande [1] proposed $D_h > 3$ mm for the conventional channels, $200 \mu\text{m} < D_h < 3$ mm for the mini-channels, and $10 \mu\text{m} < D_h < 200 \mu\text{m}$ for the micro-channels. On the other hand, Kew and Cornwell [2] introduced a dimensionless group named as the Confinement number, $N_{\text{conf}} = \frac{(\sigma/(g\Delta\rho))^{0.5}}{D_h}$, which represents the importance of the restriction of the flow by the small size of the channel. They showed that when $N_{\text{conf}} > 0.5$, the effects of the channel size became very important.

* Corresponding author. Tel.: +886 35 712121; fax: +886 35 726440.
E-mail address: tflin@mail.nctu.edu.tw (T.F. Lin).

Nomenclature

A_s	outside surface area of the heated inner pipe, m^2	Pr	Prandtl number, $Pr = \frac{\mu \cdot c_p}{k}$, dimensionless
Bo	Boiling number, $Bo = \frac{q}{G \cdot i_{fg}}$, dimensionless	q	average imposed heat flux, W/m^2
c_p	specific heat, $J/kg \cdot ^\circ C$	q_b, q_c, q_t	heat flux due to bubble nucleation, single-phase convection, total value, W/m^2
D_i, D_o	inner and outside diameters of duct, m	Q_n	net power input, W
D_h	hydraulic diameter, m, $D_h = (D_o - D_i)$	Re_l	Reynolds number of liquid in two-phase flow, $Re_l = \frac{G D_h (1-x)}{\mu_l}$, dimensionless
D_p	dimensionless mean bubble departure diameter	T_w	wall temperature of heated inner pipe, $^\circ C$
d_p	bubble departure diameter, m	T_{sat}	saturated temperature of the refrigerant, $^\circ C$
F_d	dimensionless mean bubble departure frequency	x	vapor quality
f	bubble departure frequency	z	coordinate (downstream coordinate for annular duct flow), mm
f_f	friction factor		
g	acceleration due to gravity, m/s^2		
G	mass flux, $kg/m^2 \cdot s$		
h_r	boiling heat transfer coefficient, $W/m^2 \cdot ^\circ C$		
i_{fg}	enthalpy of vaporization, J/kg		
k_l	liquid thermal conductivity, $W/m \cdot ^\circ C$		
n_{ac}	active nucleation site density, n/m^2		
N_{AC}	dimensionless active nucleation site density		
N_{conf}	confinement number, $N_{conf} = \frac{(\sigma / (g \Delta \rho))^{0.5}}{D_h}$, dimensionless		
Nu	Nusselt number, $Nu = \frac{h D_h}{k}$, dimensionless		
P	system pressure, kpa		

Greek symbols

ΔT_{sat}	wall superheat, $(T_w - T_{sat})$, $^\circ C$
δ	gap size, mm
μ_l	viscosity of liquid R-134a, $N \cdot s/m^2$
ρ_g, ρ_l	vapor and liquid densities, kg/m^3
$\Delta \rho$	density difference, $\Delta \rho = \rho_l - \rho_g$, kg/m^3
σ	surface tension, N/m

Flow boiling of refrigerants R-11 and R-123 in a horizontal small copper tube ($D_h = 1.95$ mm) investigated by Bao et al. [3] showed that the heat transfer coefficients were independent of the refrigerant mass flux and vapor quality, but were a strong function of the wall heat flux. Nucleate boiling was noted to be the dominant mechanism over a wide range of the tested flow conditions. Tran et al. [4] examined flow boiling of refrigerant R-12 in small circular and rectangular channels ($D_h = 2.46$ and 2.4 mm). Two distinct two-phase flow regions were noted, the convective boiling dominant region at lower wall superheat (< 2.75 K) and nucleate boiling dominant region at higher wall superheat (> 2.75 K). The differences in the boiling heat transfer coefficients in the circular and rectangular tubes are small. The R-134a experimental data taken from an upward vertical rectangular multi-channel ($D_h = 2.01$ mm) by Agostini and Bontemps [5] concluded that bubble nucleation was the dominant mechanism for the heat flux higher than 14 kW/m^2 and wall superheat higher than 3 K, and the transition from the boiling dominated by bubble nucleation to convection occurred at $Bo \cdot (1-x) \approx 2.2 \times 10^{-4}$. Kandlikar and Steinke [6] found that for a high liquid-to-vapor density ratio, the convective effects dominated as the vapor quality increased. This led to an increasing trend in the boiling heat transfer coefficient at increasing vapor quality. A high boiling number results in a higher nucleate boiling contribution, which tends to decrease as the vapor quality increases, causing a decreasing trend in heat transfer coefficient with increasing vapor quality. An experimental study for the flow boiling of refrigerant R-141b in a vertical tube ($D_h = 1$ mm) conducted by Lin et al. [7] con-

cluded that at low vapor quality nucleate boiling dominated. But at higher vapor quality convective boiling dominates. In a review article Watel [8] concluded that convective boiling dominated at low heat fluxes and wall superheats and high vapor qualities, otherwise nucleate boiling dominated.

To elucidate the flow boiling heat transfer mechanisms in small channels, we need to delineate the prevailing two-phase flow regimes. Cornwell and Kew [9] examined various flow regimes for boiling of refrigerant R-113 in a vertical rectangular multi-channel with $D_h = 1.03$ and 1.64 mm. Based on visualization of the boiling flow and measurement of the heat transfer, three flow regimes have been suggested, namely, the isolated bubble, confined bubble and annular-slug bubble flows. In the isolated bubble regime, the heat transfer coefficient depends on the heat flux and hydraulic diameter. In the confined bubble regime, the heat transfer coefficient depends on the mass flux and vapor quality. While in the annular-slug bubble regime, heat transfer coefficient is a function of the mass flux, vapor quality and hydraulic diameter.

It has been known for some time that bubble characteristics such as bubble departure frequency, growth, sliding and departure size play an important role in flow boiling heat transfer. Yin et al. [10] examined some bubble characteristics associated with subcooled flow boiling of refrigerant R-134a in a horizontal annular duct ($D_h = 10.31$ mm). They noted that the bubble departure frequency was suppressed by raising the mass flux and subcooling of R-134a, and only the liquid subcooling significantly affected the bubble size. Visualization of subcooled flow boiling of upward water flow in a

vertical annular channel ($D_h = 19$ mm) by Situ et al. [11] suggested that generally the bubble departure frequency increased with the heat flux and the bubble growth rate dropped sharply after the bubble lift-off. The study of water boiling in a horizontal rectangular channel with one side heated ($D_h = 40$ mm) conducted by Maurus et al. [12] manifested that the waiting time between two bubble cycles decreased significantly at increasing mass flux. Chang et al. [13] studied the near-wall bubble behavior for water in a vertical one-side heated rectangular channel ($D_h = 4.44$ mm). They showed that the size of coalesced bubbles decreased for an increase in the water mass flux and the mass flux only exhibits a strong effect on the bubble size. Del Balle and Kenning [14] examined the subcooled flow boiling for water in a rectangular vertical channel and found that the maximum bubble diameter was independent of the heat flux. An experimental study on the bubble rise path after its departure from a nucleation site for water in a vertically upward tube ($D_h = 20$ mm) by Okawa et al. [15] suggested that the inertia force significantly influenced the onset of bubble detachment and the shear force induced a lift force to detach the bubble from the wall.

An early general empirical correlation model for flow boiling in channels was proposed by Chen [16]. He divided the boiling heat transfer coefficient into two parts: a microconvective (nucleate boiling) contribution estimated by the pool boiling correlations and a macroconvective (non-boiling forced convection) contribution estimated by the single-phase correlation such as the Dittus–Boelter equation [17]. In order to account for the diminished contribution of nucleate boiling as the forced convective effects increased at a higher vapor quality, he introduced an enhancement factor E and a suppression factor S to respectively accommodate the forced convection augmentation and nucleate boiling retardation. Gungor and Winterton [18] modified the Chen's correlation and proposed the correlations for the enhancement and suppression factors. An improved correlation from Liu and Winterton [19] introduced an asymptotic function to predict the heat transfer coefficient for vertical and horizontal flows in tubes and annuli. Later Zhang et al. [20] modified the Chen's correlation to predict the heat transfer in mini channels. Besides, Tran et al. [4] modified the heat transfer correlation of Lazarek and Black [21] with the Reynolds number of the flow replaced by the Weber number to eliminate viscous effects in favor of the influences from the surface tension. Similar correlations were proposed by Fujita et al. [22].

Kandlikar [23] proposed a general correlation for saturated flow boiling heat transfer inside horizontal and vertical tubes. The correlation is also based on a model similar to that of Chen [16]. In a following study [24,25], he developed correlations to predict transition, laminar and deep laminar flows in mini-channels and micro-channels. A new correlation for boiling heat transfer in small diameter channels was proposed by Kew and Cornwell [9]. The correlation was divided by the three two-phase flow regimes based on the values of the Confinement number.

The above literature review clearly indicates that the flow boiling heat transfer of HFC refrigerants in small diameter channels remains largely unexplored. In a recent study [26,27] we report experimental data for the saturated and subcooled flow boiling heat transfer of refrigerant R-134a and associated bubble characteristics in a horizontal narrow annular duct. In the present study we move further to investigate the R-407C saturated flow boiling in the same duct. Data from this study for R-407C will be compared with those for R-134a reported in the previous study [26] and with some existing correlations for small diameter channels proposed in the open literature.

2. Experimental apparatus and procedures

The experimental system modified slightly from that used in the previous study [26] is employed here to investigate the saturated flow boiling heat transfer of R-407C in a narrow annular duct. It is schematically depicted in Fig. 1. The experimental apparatus consists of three main loops, namely, a refrigerant loop, a water-glycol loop, and a hot-water loop. Refrigerant R-407C is circulated in the refrigerant loop. In order to control various test conditions of the refrigerants in the test section, we need to control the temperature and flow rate in the other two loops.

The test section of the experimental apparatus is a horizontal annular duct with the outer pipe made of Pyrex glass to permit the visualization of boiling processes in the refrigerant flow. The glass pipe is 160-mm long with an inside diameter of 20.0 mm. Its wall is 4.0-mm thick. Both ends of the pipe are connected with copper tubes of the same size by means of flanges and are sealed by O-rings. The inner copper pipe has 16.0 or 18.0-mm nominal outside diameter with its wall being 1.5 or 2.5-mm thick and is 0.41-m long. Thus the gap of the annular duct is 2.0 or 1.0 mm ($D_h = 4.0$ or 2.0 mm). In order to insure the gap between the inner and outer pipes being uniform, we first measure the outside diameter of the inner pipe and the inside diameter of the glass pipe by digital calipers whose resolutions are 0.001 mm with the measurement accuracy of ± 0.01 mm. Then we photo the top and side view pictures of the annular duct and measure the average radial distance between the inside surface of the glass pipe to the outside surface of the inner tube. From the above procedures the duct gap is ascertained and its uncertainty is estimated to be 0.02 mm. An electric cartridge heater of 160 mm in length and 13.0 mm in diameter with a maximum power output of 800 W is inserted into the inner pipe. Furthermore, the pipe has an inactive heating zone of 10-mm long at each end and is insulated with Teflon blocks and thermally nonconducting epoxy to minimize heat loss from it. Thermal contact between the heater and the inner pipe is improved by coating a thin layer of heat-sink compound on the heater surface before the installation of the heater. Then, eight T-type calibrated thermocouples are electrically insulated by electrically nonconducting thermal bond before they are fixed on the

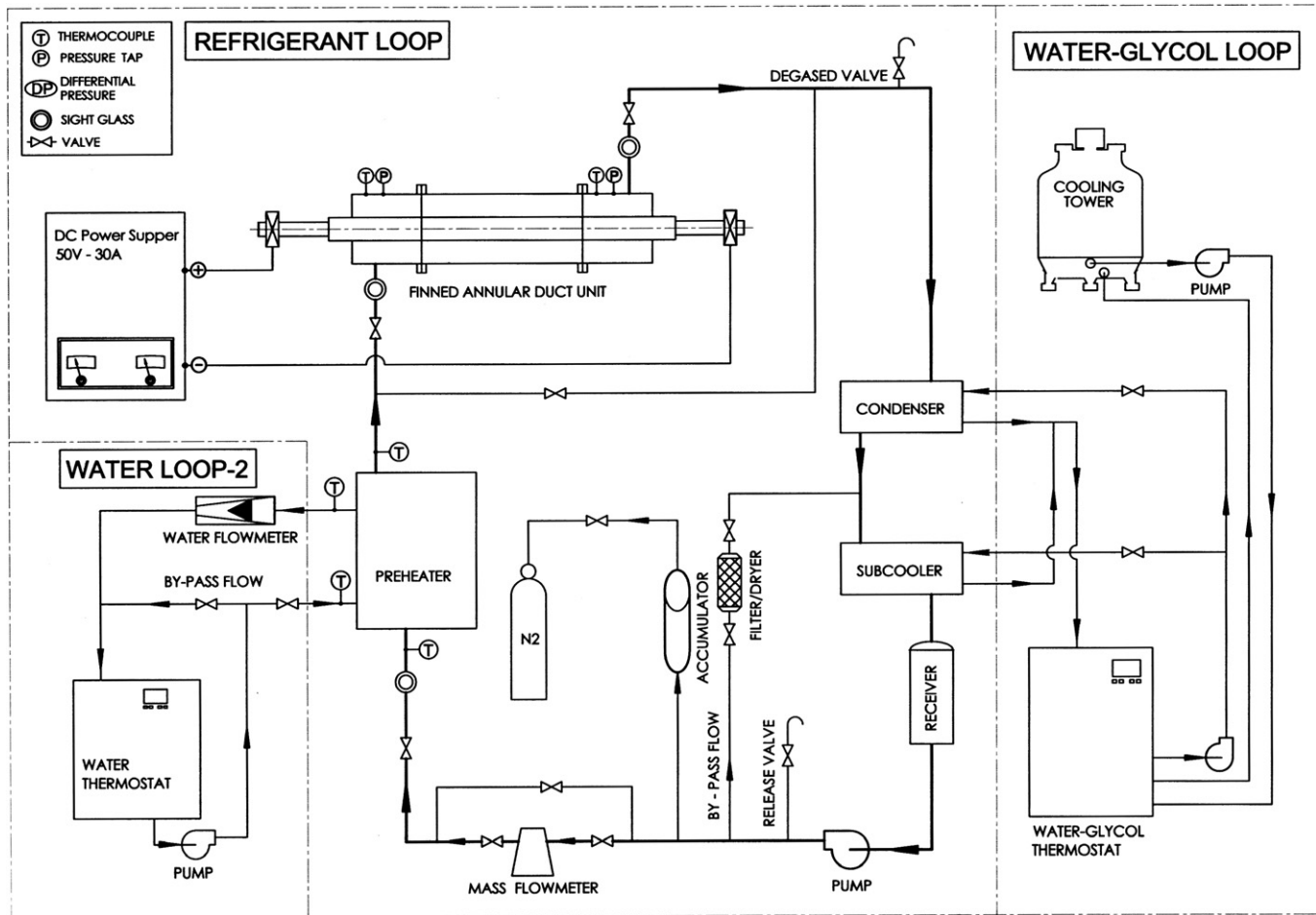


Fig. 1. Schematic of experimental system for the annular duct.

inside surface of the inner pipe so that the voltage signals from the thermocouples are not interfered with the DC current passing through the cartridge heater. The thermocouples are positioned at three axial stations along the inner pipe. At each axial station, two to four thermocouples are placed at top, bottom, or two sides of the pipe circumference with 180° or 90° apart. The outside surface temperature of the inner pipe T_w is then derived from the measured inside surface temperature by taking into account the radial heat conduction through the pipe wall.

The photographic apparatus established in the present study to record the bubble characteristics in the saturated flow boiling in the annular duct consists of an IDT X-Stream™ VISION XS-4 high speed CMOS digital camera, a Mitutoyo micro lens set, a 3D positioning mechanism, and a personal computer. The high-speed digital camera can take photographs up to 143,307 frames/s with an image resolution of 512×16 . Here, a recording rate of 10,000 frames/s with the highest image resolution of 512×256 is adopted to obtain the images of the bubble ebullition processes in the flow boiling. The data for some bubble characteristics are collected in the regions around the middle axial location ($z = 80$ mm). Note that the symbol z denotes the axial coordinate measuring from the inlet

of the heated test section. After the experimental system reaches a statistically steady state, we start recording the boiling activity. The high-speed digital camera can store the images which are later downloaded to the personal computer. Then, the mean bubble departure diameter and frequency and mean active nucleation site density are calculated by viewing more than 1000 frames at each location.

Before a test is started, the temperature of refrigerant R-407C in the test section is compared with its saturation temperature corresponding to the measured saturation pressure and the allowable difference is kept in the range of 0.2–0.3 K. Otherwise, the system is re-evacuated and then re-charged to remove the air existing in the refrigerant loop. A vacuum pump is used to evacuate noncondensable gases in the system to a low pressure of 0.067 pa in the loop. In the test the liquid refrigerant at the inlet of the test section is first maintained at the saturated state by adjusting the water-glycol temperature and flow rate. In addition, we adjust the thermostat temperature in the water loop to stabilize the refrigerant temperature at the test section inlet. Then, we regulate the refrigerant pressure at the test section inlet by adjusting the opening of the gate valve locating right after the exit of the test section. Meanwhile, by chang-

ing the current of the DC motor connecting to the refrigerant pump, the refrigerant flow rate can be varied. The imposed heat flux from the heater to the refrigerant is adjusted by varying the electric current delivered from the DC power supply. By measuring the current delivered to and voltage drop across the heater and by photographing the bubble activity, we can calculate the heat transfer rate to the refrigerant and obtain the bubble characteristics. All tests are run at statistically steady-state conditions. The whole system is considered to be at a statistically steady state when the time variations of the system pressure and imposed heat flux are respectively within $\pm 1\%$ and $\pm 4\%$, and the time variations of the heated wall temperature are less than $\pm 0.2\text{ }^\circ\text{C}$ for a period of 100 min. Then all the data channels are scanned every 0.5 s for a period of 20 s.

3. Data reduction and verification of experimental system

The imposed heat flux to the refrigerant flow in the annular duct is calculated on the basis of the net power input Q_n and the total outside surface area of the inner pipe of the annular duct A_s . The total power input Q_t is obtained from the product of the measured voltage drop across the cartridge heater and electric current passing through it. Hence the net power input to the test section is equal to $(Q_t - Q_{\text{loss}})$. The imposed heat flux at the outside surface of the inner pipe is then evaluated from the relation

$$q = Q_n / A_s \quad (1)$$

The total heat loss from the test section Q_{loss} is evaluated from the correlation for natural convection around a circular cylinder by Churchill and Chu [28]. To reduce the heat loss from the test section, it is covered with a polyethylene insulation layer. The results from this heat loss test indicate that the total heat loss from the test section is generally less than 1% of the total power input no matter when single-phase flow or two-phase boiling flow is in the duct. The saturated flow boiling heat transfer coefficient at a given axial location is defined as

$$h_r = \frac{Q_n / A_s}{(T_w - T_{\text{sat}})} \quad (2)$$

Uncertainties of the measured heat transfer coefficients are estimated according to the procedures proposed by Kline and McClintock [29] for the propagation of errors in physical measurement. The results from this uncertainty analysis are summarized in Table 1.

In order to check the suitability of the experimental system for measuring the flow boiling heat transfer coefficients, the single-phase liquid R-407C heat transfer data for the liquid Reynolds number ranging from 3459 to 14,640 are measured first and compared with the well-known traditional forced convection correlations proposed by Gnielinski [30], as that in the previous study [26,27]. The results manifest that the present data can be well correlated by their correlation with a mean absolute error of 3.9%.

Table 1
Summary of the uncertainty analysis

Parameter	Uncertainty
Annular pipe geometry	
Length, width and thickness (%)	$\pm 1.0\%$
Area (%)	$\pm 2.0\%$
Parameter measurement	
Temperature, T ($^\circ\text{C}$)	± 0.2
Temperature difference, ΔT ($^\circ\text{C}$)	± 0.3
System pressure, P (kPa)	± 2
Mass flux of refrigerant, G (%)	± 2
Saturated flow boiling heat transfer	
Imposed heat flux, q (%)	± 4.5
Heat transfer coefficient, h_r (%)	± 14.5

Thus the established system is considered to be suitable for the present R-407C flow boiling experiment.

4. Results and discussion

The present R-407C flow boiling experiments are performed for the refrigerant mass flux G varying from 300 to 600 $\text{kg/m}^2\text{ s}$, imposed heat flux q from 0 to 45 kW/m^2 , and system pressure P set at 776 kPa and 899 kPa (corresponding to the R-407C saturation temperature $T_{\text{sat}} = 10\text{ }^\circ\text{C}$ and $15\text{ }^\circ\text{C}$) for the gap of the duct $\delta = 1.0$ and 2.0 mm. The ranges of the parameters chosen above are in accordance with some air-conditioning applications. The measured boiling heat transfer data are expressed in terms of the boiling curves and boiling heat transfer coefficient. Moreover, selected flow photos and data deduced from the images of the boiling processes taken at a small region around the middle axial station $z = 80$ mm are presented to illustrate the bubble characteristics in the boiling flow. Finally, comparison with some existing correlations is made and empirical correlations to correlate the present data are proposed.

4.1. Saturated flow boiling curves

The effects of the experimental parameters including the R-407C refrigerant mass flux and saturated temperature and the gap size of the duct on the boiling curves measured at the middle axial location ($z = 80$ mm) of the narrow annular duct are illustrated in Fig. 2. The results in Fig. 2 indicate that at a low imposed heat flux the wall superheat of the heating surface is lower than that required for the onset of nucleate boiling (ONB) and no bubble nucleates from the heating surface. The flow is in single-phase state. As the imposed wall heat flux is raised gradually, the wall superheat increases correspondingly. At a certain wall superheat bubbles start to nucleate from the heating surface and we have ONB in the flow. Beyond the ONB there is a significant increase in the slope of the boiling curves, implying that a small rise in the wall superheat causes a large increase in the heat transfer rate from

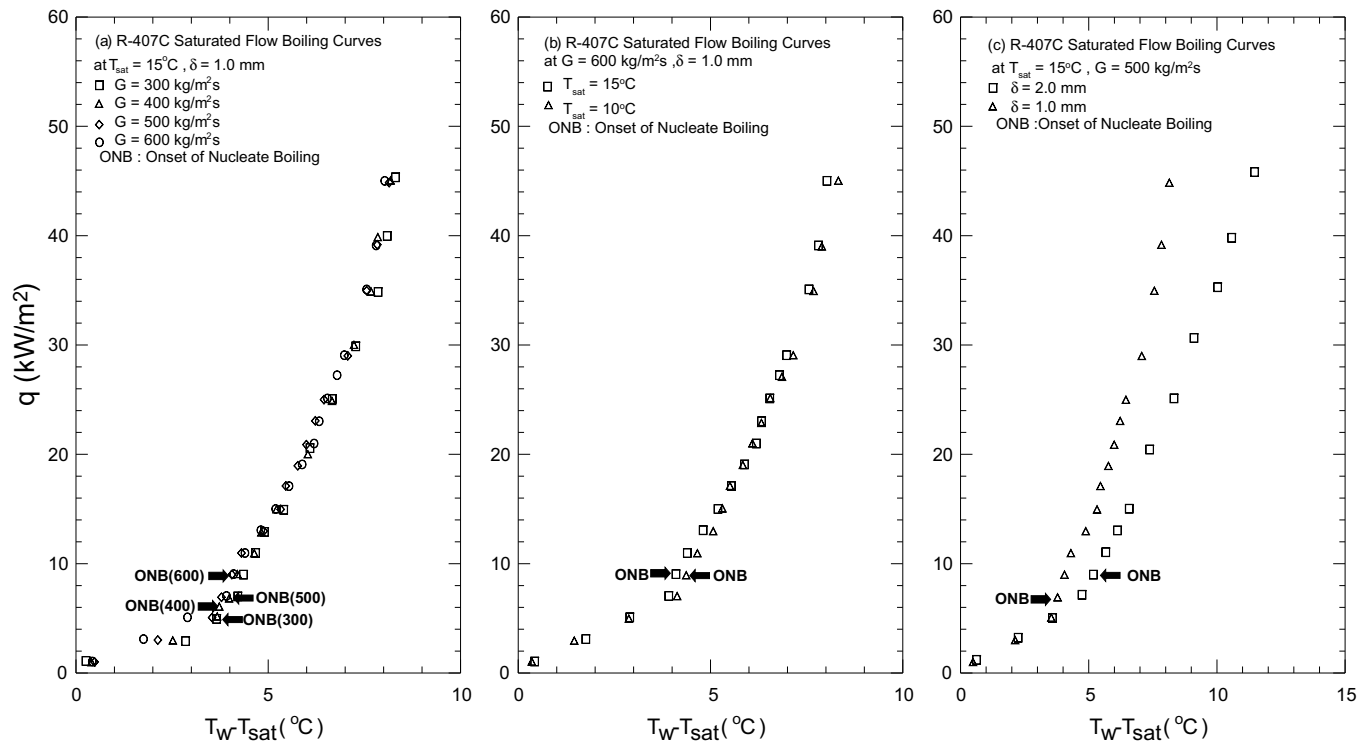


Fig. 2. Saturated flow boiling curves of R-407C: (a) for various refrigerant mass fluxes at $T_{\text{sat}} = 15^\circ\text{C}$ and $\delta = 1\text{ mm}$, (b) for various saturated temperatures at $G = 600\text{ kg/m}^2\text{ s}$ and $\delta = 1\text{ mm}$, and (c) for various gap sizes at $T_{\text{sat}} = 15^\circ\text{C}$ and $G = 500\text{ kg/m}^2\text{ s}$.

the wall to refrigerant. Note that beyond ONB the boiling curves are only slightly affected by the refrigerant mass flux (Fig. 2a), suggesting that the heat transfer is dominated by the bubble nucleation on the heating surface. But the required imposed heat flux and wall superheat to achieve ONB are influenced noticeably by the change in the mass flux. Specifically, the required imposed heat flux and wall superheat to achieve ONB are slightly higher for a higher mass flux due to the thinner thermal boundary layer. Then, the data shown in Fig. 2b indicate that the boiling curves shift slightly to the right for a reduction in the refrigerant saturated temperature. Besides, the wall superheat at ONB is not noticeably affected by T_{sat} . Finally, the effects of the duct size on the saturated flow boiling curves are shown in Fig. 2c. It is noted that the boiling curve shifts significantly to the left as the duct gap is reduced, indicating that the boiling heat transfer in the smaller duct is substantially better. It is also evident from the data that much lower imposed heat flux and wall superheat are needed to initiate boiling on the heated surface for the smaller duct. This mainly results from the fact that for given G , q and T_{sat} the mass flow rate through the duct is lower for a smaller gap. For the lower refrigerant mass flow rate the axial temperature rise of the heated surface is faster, which, in turn, causes earlier bubble nucleation for a smaller gap.

4.2. Saturated flow boiling heat transfer coefficients

The saturated flow boiling heat transfer coefficients of R-407C measured at the middle axial location

($z = 80\text{ mm}$) in the narrow annular duct affected by the three experimental parameters are shown in Fig. 3. The results indicate that at given G , δ and T_{sat} the R-407C saturated boiling heat transfer coefficient increases substantially with the imposed heat flux. For example, at $T_{\text{sat}} = 15^\circ\text{C}$, $\delta = 1.0\text{ mm}$ and $G = 500\text{ kg/m}^2\text{ s}$, the saturated boiling heat transfer coefficient for $q = 45\text{ kW/m}^2$ is about 148% higher than that for $q = 9\text{ kW/m}^2$ (Fig. 3a). This large increase in h_r is ascribed to the higher active nucleation site density on the heating surface, higher bubble departure frequency and faster bubble growth for a higher imposed heat flux. The data shown in Fig. 3a and b suggest that the saturation temperature and mass flux of the refrigerant exhibits relatively weak effects on the boiling heat transfer coefficient. Then, the results in Fig. 3c indicate that the saturated boiling heat transfer increases noticeably with a decrease in the channel gap. For example, at $q = 45\text{ kW/m}^2$, $T_{\text{sat}} = 15^\circ\text{C}$ and $G = 500\text{ kg/m}^2\text{ s}$ the saturated boiling heat transfer coefficient for $\delta = 1.0\text{ mm}$ is about 38% higher than that for $\delta = 2.0\text{ mm}$ (Fig. 3c). Since the shear stress of the flow acting on the heated surface in a smaller channel is higher, the bubbles on the heating surface can be more easily swept away from the heated surface. Moreover, the flow pattern change from a bubbly flow to a slug flow for $\delta = 1.0\text{ mm}$ occurs at a lower imposed heat flux than that for $\delta = 2.0\text{ mm}$. These effects are thought to be the main reasons for the enhancement of flow boiling heat transfer when the channel size is reduced.

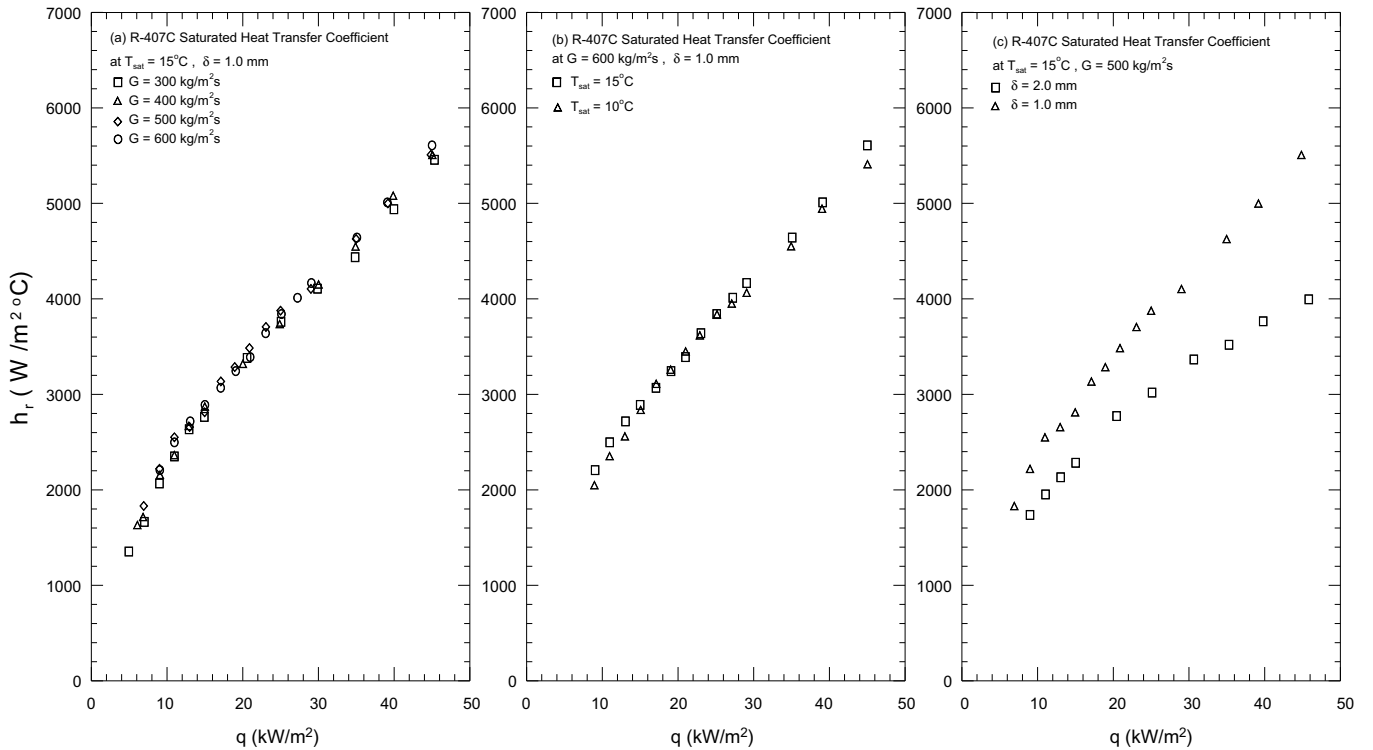


Fig. 3. Saturated flow boiling heat transfer coefficient of R-407C: (a) for various refrigerant mass fluxes at $T_{sat} = 15\text{ }^\circ\text{C}$ and $\delta = 1\text{ mm}$, (b) for various saturated temperatures at $G = 600\text{ kg/m}^2\text{ s}$ and $\delta = 1\text{ mm}$, and (c) for various gap sizes at $T_{sat} = 15\text{ }^\circ\text{C}$ and $G = 500\text{ kg/m}^2\text{ s}$.

4.3. Bubble characteristics in saturated flow boiling

The photos of the R-407C boiling flow for the cases at different refrigerant mass fluxes, duct size, saturated tem-

perature and imposed heat fluxes taken from a small region around the middle axial location are shown in Fig. 4. First of all, it is noted from the photo taken from the duct for $\delta = 1.0\text{ mm}$ shown in Fig. 4a for the case at $T_{sat} = 15\text{ }^\circ\text{C}$

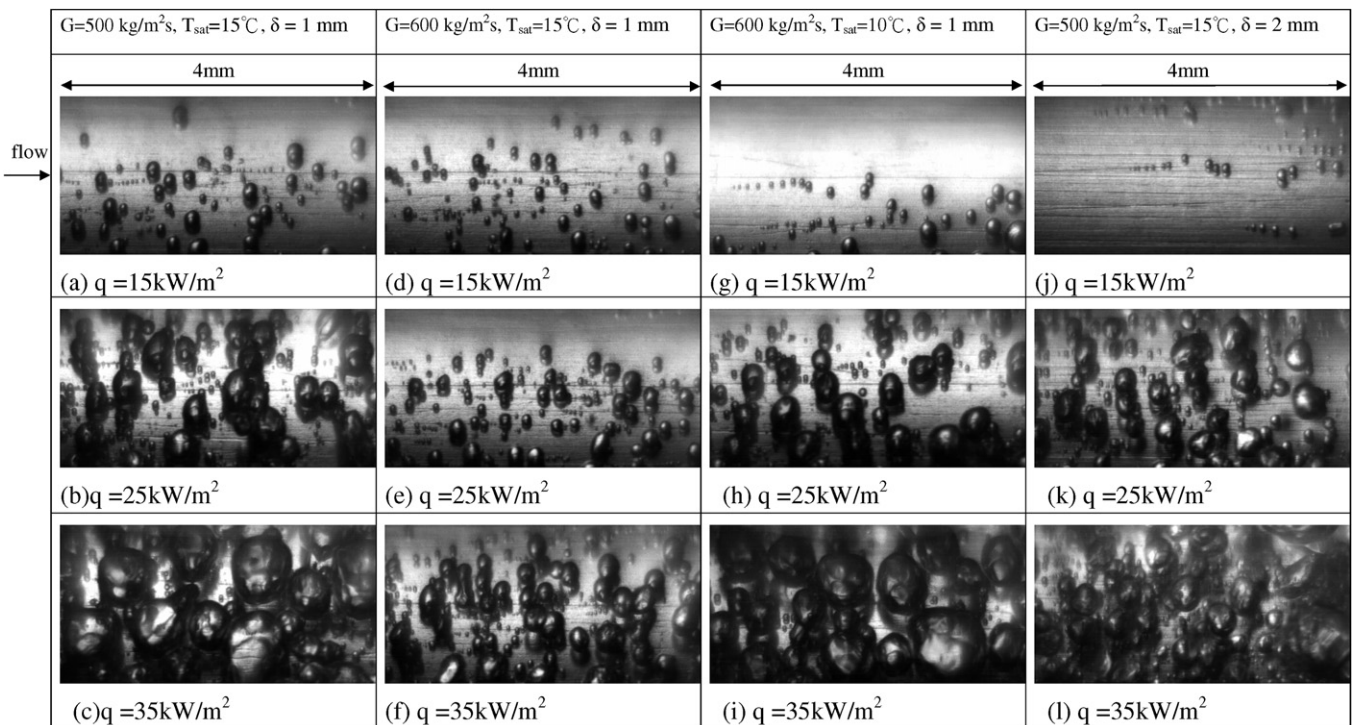


Fig. 4. Photos of bubbles in the saturated flow boiling of R-407C in a small region around middle axial location at $T_{sat} = 15\text{ }^\circ\text{C}$ for various imposed heat flux, mass fluxes, saturated temperature and gap sizes.

and $G = 500 \text{ kg/m}^2 \text{ s}$ at the imposed heat flux $q = 15 \text{ kW/m}^2$ that a number of discrete bubbles nucleate from the cavities and slide along the heating surface. As the imposed heat flux is increased to $q = 25 \text{ kW/m}^2$, the active bubble nucleation density increases and a lot of coalescence bubbles appear (Fig. 4b). More coalescence bubbles are seen and they are confined by the duct walls to become slightly deformed as the heat flux is raised to $q = 35 \text{ kW/m}^2$ (Fig. 4c). At even higher heat fluxes the duct is filled with the coalescence bubbles. The results in Fig. 4a–f indicate that at a higher refrigerant mass flux the liquid refrigerant moves at a higher speed, which in turn tends to sweep the bubbles more quickly away from the heating surface. Besides, the bubble departure frequency is higher and the bubbles are smaller and in violent agitating motion. However, at the higher liquid speed the residence time of the refrigerant on the heating surface is shorter and the liquid is heated to a lower temperature, resulting in a smaller active nucleation site density at a higher mass flux. Note that at the lower mass flux the bubble coalescence is more important and a number of bigger bubbles form in the duct. Then, the effects of the refrigerant saturation temperature on the bubble characteristics are illustrated by comparing the photos in Fig. 4d–f with Fig. 4g–i. The results indicate that at a lower saturation temperature the bubbles grow bigger and depart at a lower rate, and the active nucleation site density is lower due to the higher surface tension and enthalpy of vaporization. Finally, the effects of the duct size on the bubble characteristics are illustrated

by comparing the photos in Fig. 4a–c with Fig. 4j–l. It is noted that more bubbles appear in the narrower duct at the imposed heat flux $q = 15 \text{ kW/m}^2$ (Fig. 4a and j). As the imposed heat flux is increased to $q = 25 \text{ kW/m}^2$ (Fig. 4b and k), in the smaller duct the bubble departure frequency is higher and the bubbles collide and coalesce more frequently due to the less space available for the boiling flow (the confinement effect). As the heat flux is raised to $q = 35 \text{ kW/m}^2$ (Fig. 4c and l), large coalesced bubbles dominate in the smaller duct. For a further increase in the imposed heat flux, the flow pattern in the middle portion of the smaller duct changes from a bubbly flow regime to a slug flow regime.

To be more quantitative on the bubble characteristics, we estimate the average bubble departure diameter and frequency and the number density of the active nucleation sites on the heating surface from the images of the boiling flow stored in the video tapes. The results from this estimation are examined in the following. The effects of the three parameters on the mean bubble departure diameter for the saturated flow boiling of R-407C at the middle axial location ($z = 80 \text{ mm}$) in the annular duct are shown in Fig. 5. First, the effects of the refrigerant mass flux shown in Fig. 5a indicate that the average departing bubble is only slightly larger for a lower refrigerant mass flux. Then, the results in Fig. 5b indicate that the average bubble departure diameter is somewhat smaller for a higher refrigerant saturated temperature. Finally, it is of interest to note from the data given in Fig. 5c that the effects of the duct gap on the

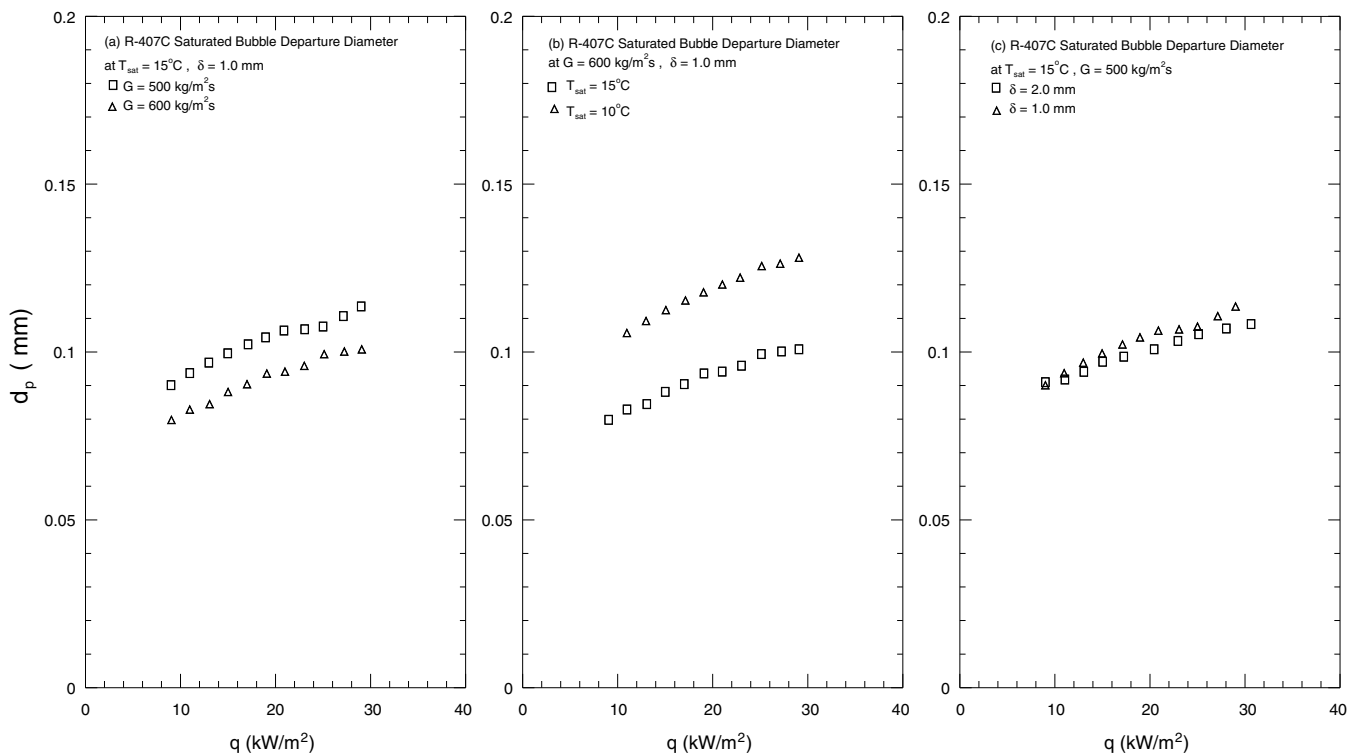


Fig. 5. Mean bubble departure diameter for saturated flow boiling of R-407C: (a) for various refrigerant mass fluxes at $T_{\text{sat}} = 15^\circ\text{C}$ and $\delta = 1 \text{ mm}$, (b) for various saturated temperatures at $G = 600 \text{ kg/m}^2 \text{ s}$ and $\delta = 1 \text{ mm}$, and (c) for various gap sizes at $T_{\text{sat}} = 15^\circ\text{C}$ and $G = 500 \text{ kg/m}^2 \text{ s}$.

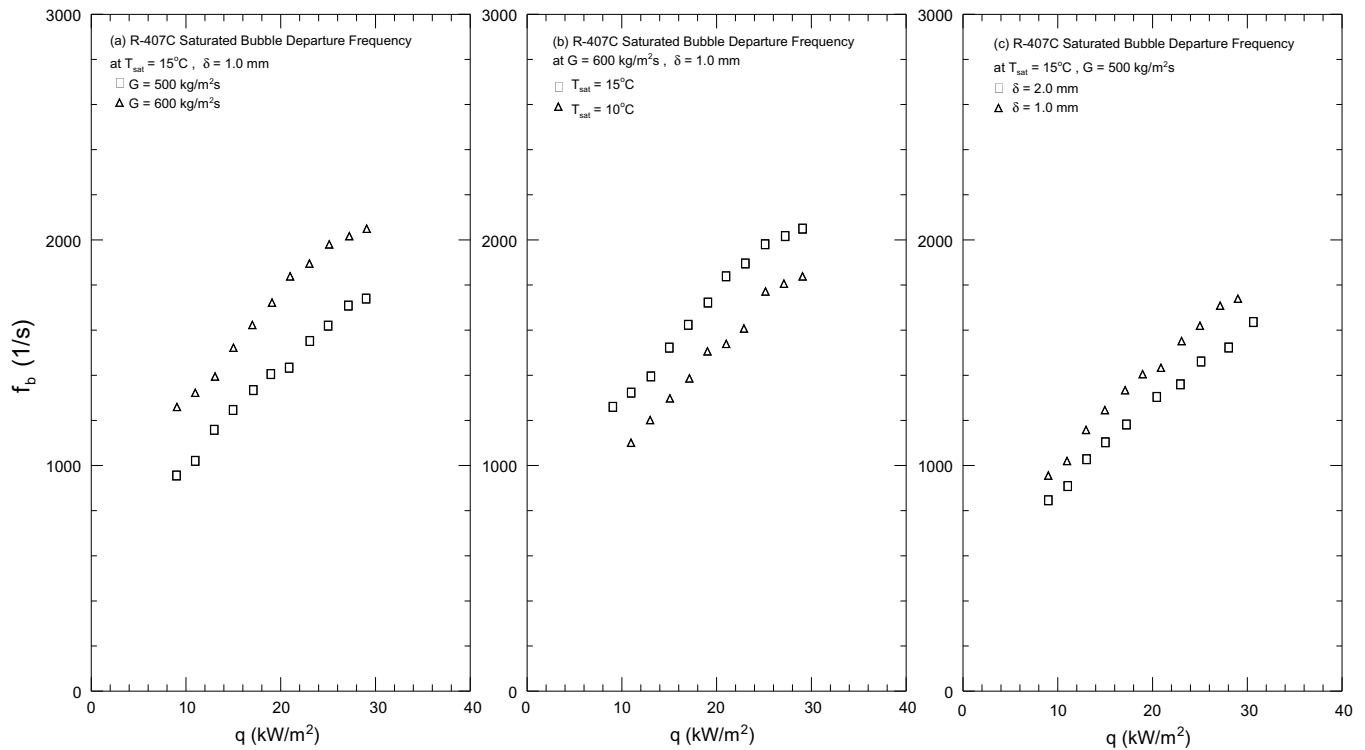


Fig. 6. Mean bubble departure frequency for saturated flow boiling of R-407C: (a) for various refrigerant mass fluxes at $T_{\text{sat}} = 15^\circ\text{C}$ and $\delta = 1\text{ mm}$, (b) for various saturated temperatures at $G = 600\text{ kg/m}^2\text{ s}$ and $\delta = 1\text{ mm}$, and (c) for various gap sizes at $T_{\text{sat}} = 15^\circ\text{C}$ and $G = 500\text{ kg/m}^2\text{ s}$.

bubble departure diameter are relatively small. Note that the departing bubble is larger at a higher imposed heat flux.

How the bubble departure frequency is affected by the three parameters for the saturated flow boiling of R-407C at the middle axial location ($z = 80\text{ mm}$) in the annular duct are shown in Fig. 6. Note that the increase of the bubble departure frequency with the imposed heat flux is rather significant for all cases presented here. Besides, the bubble departure frequency is higher with higher refrigerant mass flux and saturated temperature and smaller duct size.

The associated number density of the active nucleation sites affected by the three parameters are shown in Fig. 7. The data clearly show the substantial increase of the active nucleation site density with the imposed heat flux for all cases examined here. It is noted that the active nucleation site density is higher with lower refrigerant mass flux and higher refrigerant saturated temperature especially at high imposed heat flux. The data shown in Fig. 7c manifest that the effect of the duct gap on the R-407C average active nucleation site density is insignificant.

4.4. Comparison with data for R-134a flow boiling

We move further to compare the present data for the R-407C saturated flow boiling with the measured data for R-134a flow boiling from Lie [31] in the same narrow annular duct. The results from this comparison are illustrated in Fig. 8. The data from the boiling curves in Fig. 8 indicate that a higher imposed heat flux is needed to initiate boiling

for R-134a. This can be attributed to the lower surface tension for R-407C. Besides, the slopes of the boiling curves for R-407C are much steeper, suggesting the saturated flow boiling heat transfer for R-407C is much better. Indeed, the data in Fig. 8b manifest that R-407C has a much higher boiling heat transfer coefficient except at the low heat flux near ONB.

4.5. Comparison with some existing correlations

Moreover, the present data for the R-407C saturated flow boiling heat transfer coefficient are compared with some existing empirical correlations proposed in the open literature. The results from this comparison are shown in Fig. 9. Note that the correlation from Lazarek and Black [21] substantially overpredicts our data. Similarly, the correlations from Bao et al. [3], Tran et al. [4], Liu and Winterton [19] and Kandlikar [23] also overpredict our data to some degree. However, our data are well correlated by the correlation of Fujita et al. [22].

4.6. Correlation equations

According to flow boiling mechanisms [16], the heat transfer in the bubbly flow regime in the flow boiling can be roughly considered as a combination of single-phase liquid forced convection heat transfer q_c and pool boiling heat transfer q_b . Thus the total heat flux input to the boiling flow q_t can be expressed as

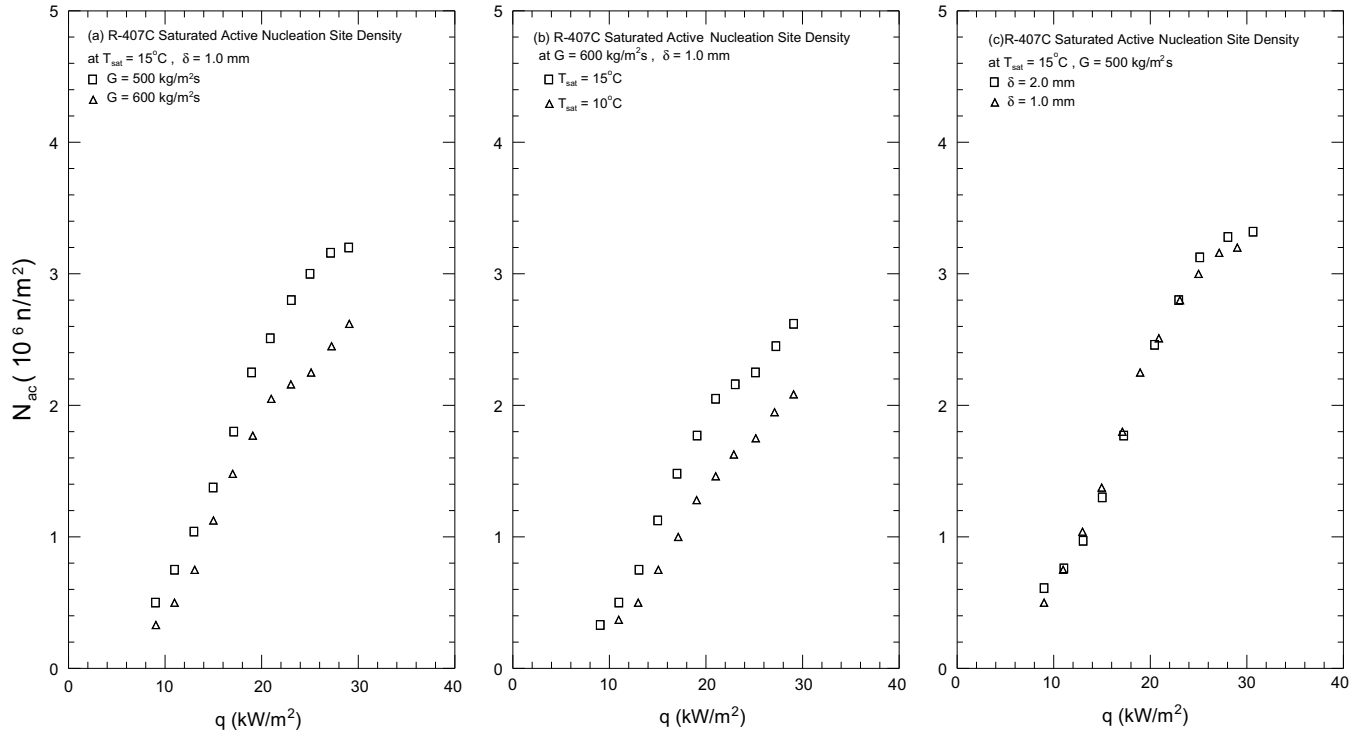


Fig. 7. Mean active nucleation site density for saturated flow boiling of R-407C: (a) for various refrigerant mass fluxes at $T_{\text{sat}} = 15^\circ\text{C}$ and $\delta = 1\text{ mm}$, (b) for various saturated temperatures at $G = 600\text{ kg/m}^2\text{ s}$ and $\delta = 1\text{ mm}$, and (c) for various gap sizes at $T_{\text{sat}} = 15^\circ\text{C}$ and $G = 500\text{ kg/m}^2\text{ s}$.

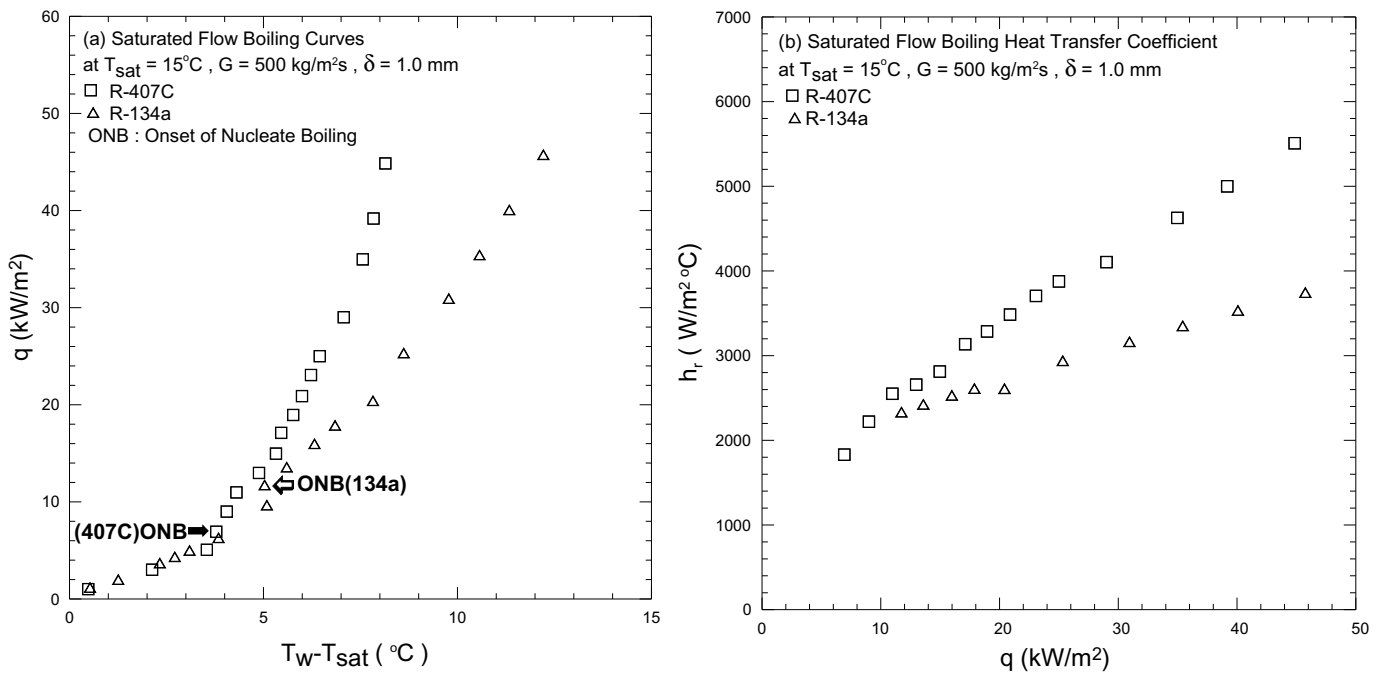


Fig. 8. Comparison between R-407C and R-134a saturated flow boiling for (a) saturated boiling curves and (b) saturated flow boiling heat transfer coefficient.

$$q_t = q_b + q_c \tag{3}$$

$$q_c = h_1 \Delta T_{\text{sat}} \tag{5}$$

Here q_b and q_c can be, respectively, calculated from the relations

$$q_b = \rho_g V_g f N_{ac} i_{fg} \tag{4}$$

and

Note that q_b expressed in Eq. (4) in fact represents the latent heat carried away from the heating surface during the departure of bubbles from the surface. The single-phase forced convection heat transfer coefficient is estimated from the correlation for the Nusselt number Nu_1 as

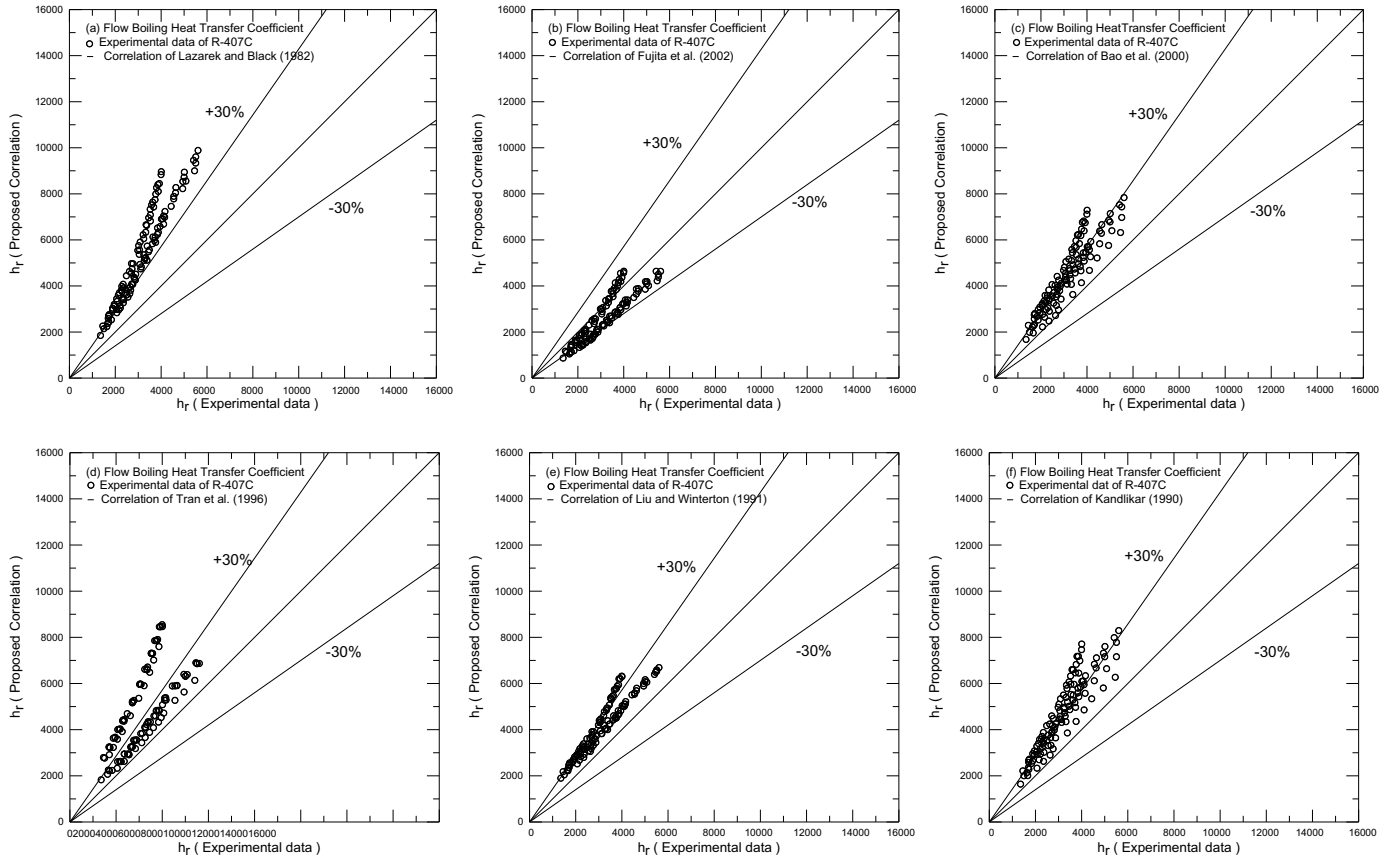


Fig. 9. Comparison of the present data for heat transfer coefficient in the saturated flow boiling of R-407C with existing correlations.

$$h_l = Nu_l k_l / D_h \quad (6)$$

and Nu_l is estimated from the Gnielinski correlation [30],

$$Nu_l = \frac{(f_f/8)(Re_l - 1000)Pr_l}{1 + 12.7\sqrt{f_f/8}(Pr_l^{2/3} - 1)} \quad (7)$$

Here the friction factor f_f is evaluated from the relation

$$f_f = (1.82 \times \log_{10} Re_l - 1.64)^{-2} \quad (8)$$

Moreover, the Reynolds number of the liquid flow is defined as

$$Re_l = GD_h(1 - x) / \mu_l \quad (9)$$

In the above equations ρ_g is the vapor density, V_g is the mean vapor volume of a departing bubble which is equal to $\frac{4\pi}{3} \left(\frac{d_p}{2}\right)^3$, f is bubble departure frequency, N_{ac} is the active nucleation site density, i_{fg} is the enthalpy of vaporization. Because the range of the experimental Re_l is between 5600 and 11,500, we use the Gnielinski correlation for $Re_l > 2300$ to estimate the single-phase convection heat transfer. It is difficult to distinguish the individual bubbles at a higher imposed heat flux since many big bubbles form due to the prominent effects of the bubble merging, which in turn overshadows the small bubbles departing from the heating surface. Hence the above correlations do not apply to the data for $q > 30 \text{ kW/m}^2$.

To enable the usage of the above correlation for the flow boiling heat transfer, the mean departing bubble size and departure frequency and the active nucleation density on the heating surface need to be correlated in advance. The average bubble departure diameter in the saturated flow boiling of R-407C in the narrow annular duct estimated from the present flow visualization can be correlated as

$$D_p = \frac{d_p}{\sqrt{\sigma/(g\Delta\rho)}} = 0.9 \left(\frac{\rho_l}{\rho_g}\right)^{0.5} Re_l^{-0.25} \cdot Bo^{0.2} \cdot N_{conf}^{-0.2} \quad (10)$$

Fig. 10a shows that almost all the present experimental data for d_p fall within $\pm 20\%$ of the above correlation and the mean absolute error is 5%. Besides, an empirical equation is proposed for the product of the mean bubble departure diameter and departure frequency as

$$F_d = \frac{f \cdot d_p}{\mu_l / (\rho_l D_h)} = 1.61 Re_l^{1.4} \cdot Pr_l^2 \cdot Bo^{0.7} \cdot N_{conf} \quad (11)$$

Note that almost all the experimental data collected in this study can be correlated within $\pm 30\%$ by Eq. (11) and the mean absolute error is 19% (Fig. 10b). Finally, we propose an empirical correlation for the average active nucleation site density in the saturated flow boiling of R-407C in the narrow annular duct as

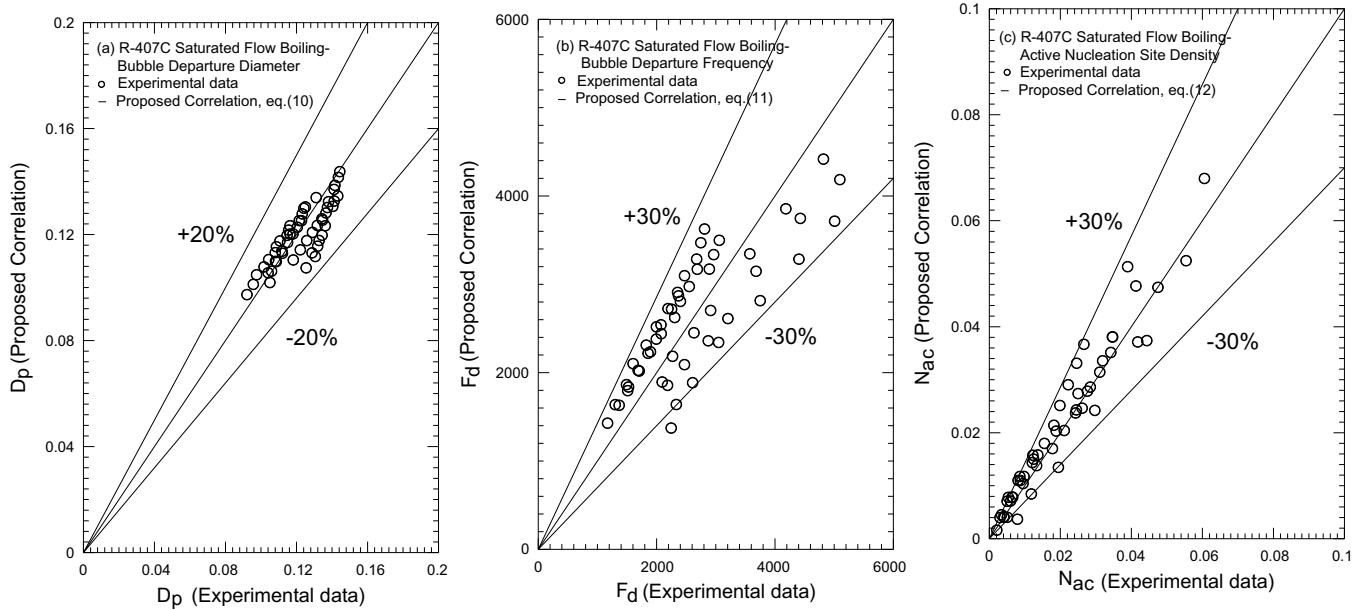


Fig. 10. Comparison of the measured data for mean bubble departure diameter: (a), mean bubble departure frequency (b), and mean active nucleation site density (c) in the saturated flow boiling of R-407C with the proposed correlations.

$$N_{AC} = n_{ac}d_p^2 = -0.009 + 1000Bo^{1.25}Re_1^{0.05}N_{conf}^{0.06} \quad (12)$$

$q > 20 \text{ kW/m}^2$ are substantially overpredicted by the above correlations.

Fig. 10c shows that the present experimental data fall within $\pm 30\%$ of the above correlation and the mean absolute error is 18%.

When the correlations for d_p , f , and n_{ac} given in Eqs. (10)–(12) are combined with Eqs. (3)–(9) for q_t , most boiling heat transfer data measured in the present study fall within $\pm 30\%$ of the correlation proposed here with the mean deviation of 20.5% (Fig. 11). Note that the data for

5. Concluding remarks

The experimental heat transfer data for the saturated flow boiling of R-407C in the narrow annular duct have been presented here. Meanwhile, the bubble behavior in the boiling flow is examined. The effects of the imposed heat flux, refrigerant mass flux, saturated temperature, and duct size on the R-407C saturated flow boiling heat transfer coefficient and associated bubble characteristics have been investigated in detail. Moreover, comparison of the present data with some existing correlations is conducted. The major results obtained here can be summarized in the following:

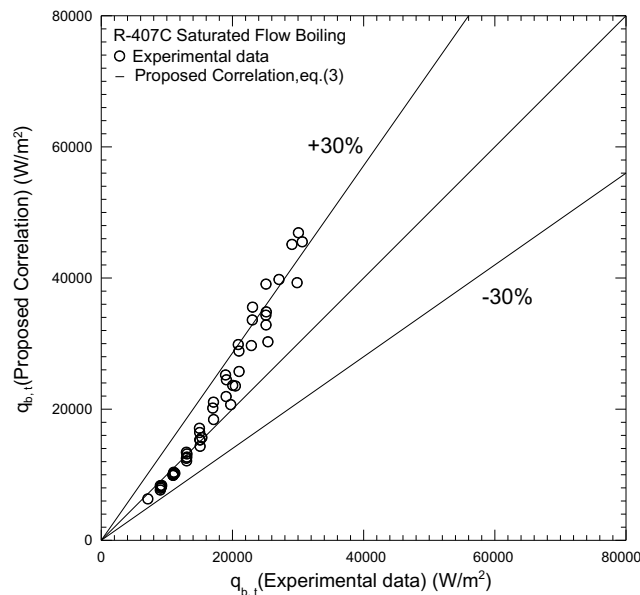


Fig. 11. Comparison of the measured data for heat transfer coefficient in the saturated flow boiling of R-407C with the proposed correlation.

- (1) The saturated boiling heat transfer coefficients increase with a decrease in the gap size. Besides, raising the imposed heat flux can cause a significant increase in the boiling heat transfer coefficient. However, the effects of the refrigerant mass flux and saturated temperature on the boiling heat transfer coefficient are small but cannot be entirely neglected in the narrow duct examined here.
- (2) The results from the flow visualization show that the mean diameter of the bubbles departing from the heating surface decreases noticeably at increasing refrigerant mass flux and saturated temperature. Besides, at a high imposed heat flux many bubbles generated from the cavities in the heating surface tend to merge together to form big bubbles. The bubble departure frequency increases with the increasing

refrigerant mass flux and saturated temperature and with the decreasing duct size. The active nucleation site density is much lower at a higher refrigerant mass flux and lower refrigerant saturation temperature especially at high imposed heat flux.

- (3) The boiling heat transfer coefficient, mean bubble departure diameter, bubble departure frequency and active nucleation site density in the R-407C saturated flow boiling are correlated in terms of the relevant dimensionless groups.

Acknowledgement

The financial support of this study by the engineering division of National Science Council of Taiwan, ROC through the contract NSC 92-2212-E-009-016 is greatly appreciated.

References

- [1] S.G. Kandlikar, W.J. Grande, Evolution of microchannel flow passages-thermohydraulic performance and fabrication technology, *Heat Transfer Eng.* 24 (1) (2003) 3–17.
- [2] P.A. Kew, K. Cornwell, Correlations for the prediction of boiling heat transfer in small-diameter channels, *Appl. Therm. Eng.* 17 (1997) 705–715.
- [3] Z.Y. Bao, D.F. Fletcher, B.S. Haynes, Flow boiling heat transfer of Freon R11 and HCFC123 in narrow passages, *Int. J. Heat Mass Transfer* 43 (18) (2000) 3347–3358.
- [4] T.N. Tran, M.W. Wambsganss, D.M. France, Small circular- and rectangular-channel boiling with two refrigerants, *Int. J. Multiphase Flow* 22 (1996) 485–498.
- [5] B. Agostini, A. Bontemps, Vertical flow boiling of refrigerant R134a in small channels, *Int. J. Heat Fluid Flow* 26 (2005) 296–306.
- [6] S.G. Kandlikar, M.E. Steinke, Flow boiling heat transfer coefficient in minichannels – correlation and trends, *Proc. 12th Int. Heat Transfer Conf.* 3 (2002) 785–790.
- [7] S. Lin, P.A. Kew, K. Cornwell, Two-phase heat transfer to a refrigerant in a 1 mm diameter tube, *Int. J. Refrigeration* 24 (1) (2001) 51–56.
- [8] B. Watel, Review of saturated flow boiling in small passages of compact heat exchangers, *Int. J. Therm. Sci.* 42 (2003) 107–140.
- [9] K. Cornwell, P.A. Kew, Boiling in small parallel channels, in: P.A. Pilavachi (Ed.), *Energy Efficiency Process Technol.*, Elsevier Applied Science, London, 1993, pp. 624–638.
- [10] C.P. Yin, Y.Y. Yan, T.F. Lin, B.C. Yang, Subcooled flow boiling heat transfer of R-134a and bubble characteristics in a horizontal annular duct, *Int. J. Heat Mass Transfer* 43 (2000) 1885–1896.
- [11] R. Situ, Y. Mi, M. Ishii, M. Mori, Photographic study of bubble behaviors in forced convection subcooled boiling, *Int. J. Heat Mass Transfer* 47 (2004) 3659–3667.
- [12] R. Maurus, V. Ilchenko, T. Sattelmayer, Automated high-speed video analysis of the bubble dynamics in subcooled flow boiling, *Int. J. Heat Fluid Flow* 25 (2004) 149–158.
- [13] S.H. Chang, I.C. Bang, W.P. Baek, A photographic study on the near-wall bubble behavior in subcooled flow boiling, *Int. J. Therm. Sci.* 41 (2002) 609–618.
- [14] V.H. Del Balle, D.B.R. Kenning, Subcooled flow boiling at high heat flux, *Int. J. Heat Mass Transfer* 28 (10) (1985) 1907–1920.
- [15] T. Okawa, T. Ishida, I. Kataoka, M. Mori, An experimental study on bubble rise path after the departure from a nucleation site in vertical upflow boiling, *Exp. Therm. Fluid Sci.* 29 (2005) 287–294.
- [16] J.C. Chen, A correlation for boiling heat transfer to saturated fluids in convective flow, *Ind. Eng. Chem. Process Des. Dev.* 5 (1966) 322–329.
- [17] F.W. Dittus, L.M.K. Boelter, *Heat Transfer Automobile Rad. Tube Type, 2*, Springer, Berkley, 1930, p. 250.
- [18] K.E. Gungor, R.H.S. Winterton, A general correlation for flow boiling in tubes and annuli, *Int. J. Heat Mass Transfer* 29 (1986) 351–358.
- [19] Z. Liu, R.H.S. Winterton, A general correlation for saturated and subcooled flow boiling in tubes and annuli, based on a nucleate pool boiling equation, *Int. J. Heat Mass Transfer* 34 (1991) 2759–2766.
- [20] W. Zhang, T. Hibiki, K. Mishima, Correlation for flow boiling heat transfer in mini-channels, *Int. J. Heat Mass Transfer* 47 (2004) 5749–5763.
- [21] G.M. Lazarek, S.H. Black, Evaporative heat transfer, pressure drop and critical heat flux in a small vertical tube with R-113, *Int. J. Heat Mass Transfer* 25 (7) (1982) 945–960.
- [22] Y. Fujita, Y. Yang, N. Fujita, Flow boiling heat transfer and pressure drop in uniformly heated small tubes, *Proc. 12th Int. Heat Transfer Conf.* 3 (2002) 743–748.
- [23] S.G. Kandlikar, A general correlation for two-phase flow boiling heat transfer coefficient inside horizontal and vertical tubes, *ASME J. Heat Transfer* 102 (1990) 219–228.
- [24] S.G. Kandlikar, A model for predicting the two-phase flow boiling heat transfer coefficient in augmented tube and compact heat exchanger geometries, *ASME J. Heat Transfer* 113 (1991) 966–972.
- [25] S.G. Kandlikar, P. Balasubramanian, An extension of the flow boiling correlation to transition, laminar, and deep laminar flows in minichannels and microchannels, *Heat Transfer Eng.* 25 (2004) 86–93.
- [26] Y.M. Lie, T.F. Lin, Saturated flow boiling heat transfer and associated bubble characteristics of R-134a in a narrow annular duct, *Int. J. Heat Mass Transfer* 48 (25–26) (2005) 5602–5615.
- [27] Y. M. Lie, T.F. Lin, Subcooled flow boiling heat transfer and associated bubble characteristics of R-134a in a narrow annular duct, *Int. J. Heat Mass Transfer* 49 (13–14) (2006) 2077–2089.
- [28] S.W. Churchill, H.H.S. Chu, Correlating equations for laminar and turbulent free convection from a horizontal cylinder, *Int. J. Heat Mass Transfer* 18 (1975) 1049–1053.
- [29] S.J. Kline, F.A. McClintock, Describing uncertainties in single-sample experiments, *ASME Mech. Eng.* 75 (1) (1953) 3–12.
- [30] V. Gnielinski, New equations for heat and mass transfer in turbulent pipe and channel flow, *Int. Chem. Eng.* 16 (2) (1976) 359–368.
- [31] Y.M. Lie, Heat transfer and bubble characteristics associated with flow boiling of refrigerant R-134a in a horizontal narrow annular duct, Ph.D thesis, National Chiao Tung University, Taiwan, 2006.